Anisotropy of optical and electrical properties of rutile SnO_2

PIs Rüdiger Goldhahn (C1.5, associate partner Magdeburg University), Zbigniew Galazka (C3.1), Oliver Bierwagen (C3.3)

Research team Martin Feneberg and Christian Lidig (Magdeburg University)

External collaborators: J.S. Speck, M.E. White, M.Y. Tsai (UCSB)

Tin dioxide or stannic oxide (rutile SnO_2) has a wide variety of applications. Prime examples are as transparent conducting oxide, as active layer in gas-sensing devices, and as heat-reflective coating on optical windows. All these examples rely on n-type doped SnO_2 with different free-electron concentrations (n) which are engineered by e.g. antimony or fluorine doping. Therefore, important electrical and optical properties for application are governed by the presence of electrons in the non-parabolic conduction band (CB) whose motion can be described by n-dependent effective electron masses [1]. The goal of this collaborative research is the determination of fundamental band structure properties, their tuning by doping, and the impact on electrical/optical behavior. In particular, the dependence on crystallographic orientation has to be considered because of the anisotropic nature of the rutile structure (properties perpendicular and parallel to the **c-axis)**.

The successful completion of this task is only possible by combining studies of high-quality bulk SnO_2 crystals (low free-electron concentrations and different orientation, IKZ) [2] and of corresponding MBE-grown epitaxial films for which $n > 10^{20}$ cm^{-3} can be realized while maintaining high-quality crystalline structure (PDI in collaboration with University of California, Santa Barbara, [3]).

Starting point is our previous joint work [1] where infrared ellipsometry was applied for determining the effective electron masses perpendicular and parallel to **c** as a function electron density (MBE-grown films). The main result is displayed in Fig. 1. We found (i) a pronounced anisotropy which becomes larger for $n > 3 \times 10^{19}$ cm^{-3}, and (ii) with n increasing effective masses (CB nonparabolicity). At low n, an effective mass anisotropy ratio of $m_\perp^*/m_\parallel^* = 1.25$ was estimated being very close to the value of 1.28 reported by Button (cyclotron resonance). In the reporting period, we demonstrated [4] an inherent electron transport anisotropy of SnO_2 being related to the effective mass anisotropy. Unintentionally doped ($n \approx 10^{18}$ cm^{-3}) bulk crystals with (100) and (110) surfaces were studied by van der Pauw measurements as a function of temperature yielding the anisotropic mobilities and their ratio as expressed via $A = \mu_\parallel/\mu_\perp$ and shown in Fig. 2. The mobility parallel to the **c**-axis is always higher than perpendicular to it over the whole temperature range. The pronounced changes below 100 K were tentatively attributed to low-angle grain boundaries with a low energy barrier. However, an almost constant ratio for A of about 1.26 is found above 250 K. It can be fully explained by the effective mass anisotropy ratio as mentioned above. Then, the result suggests rather isotropic scattering mechanisms. In conclusion, the efficiency of mobility sensitive applications, such as field effect transistors, can be increased by aligning the transport direction along the **c**-axis. For highly-doped layers, this becomes even more important because the effective mass anisotropy increases as demonstrated by us.

Fig. 1: *Effective electron masses as a function of free-electron concentration in SnO₂:Sb (symbols). Continuous curves represent an empiric model description.[1]*

Fig. 2: *(a) Mobility anisotropy A as a function of temperature for two bulk samples with (100) and (110) surface orientation. (b) Arrhenius plot of A below 100 K.[4]*
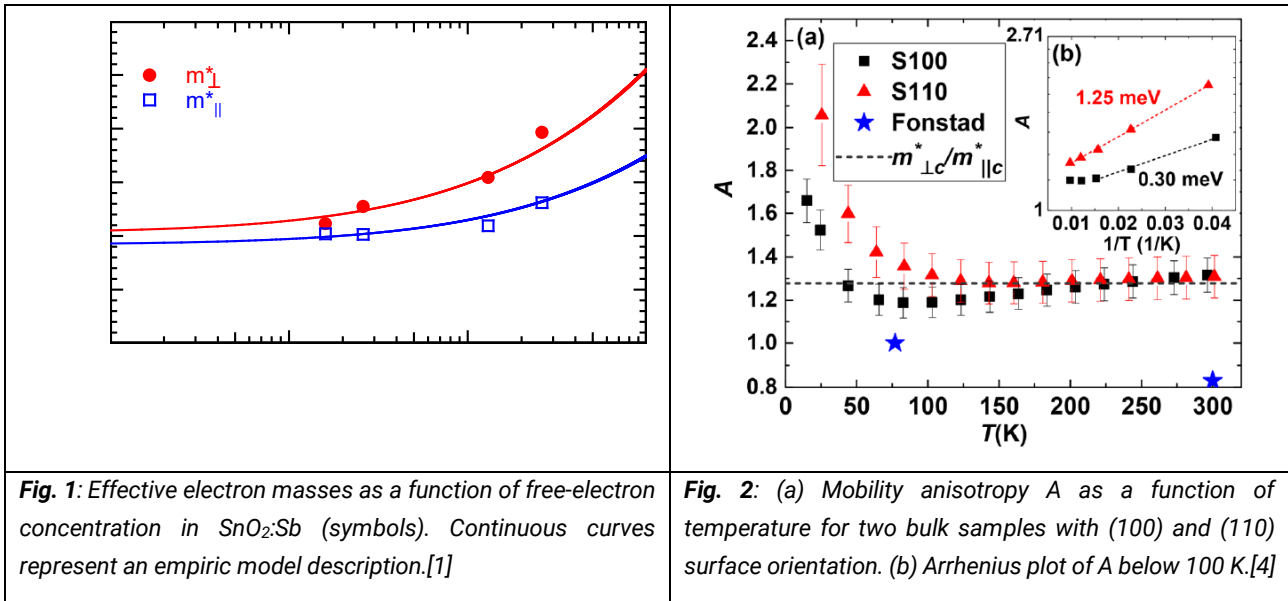
In the second part of the current project, we studied the influence of high electron densities on the optical anisotropy around the fundamental absorption edge. Starting point are again own studies [5] where we already demonstrated that combination of lab- and synchrotron-based ellipsometry in various configurations allow the determination of both, the ordinary and extraordinary dielectric tensor components up to 20 eV (MBE-grown film with low n). Theoretical calculations agree well with the experimental data if electron-hole interaction (exciton) is fully taken into account.

At first we demonstrated now [6], that the studies of either (110)-oriented bulk crystals or (101)-oriented MBE films with low n ($6\text{-}7{*}10^{17}\text{cm}^{-3}$) yield almost identical ordinary (electric field polarization perpendicular to **c**) and extraordinary (E parallel **c**) DFs around the fundamental absorption edge (data for the bulk crystal are shown in Fig. 3). Taking the excitonic nature into account, all contributions determining the shape of the absorption edges can be unambiguously identified. Direct transitions between one/two valence bands into the CB represent the main absorption processes of the ordinary/extraordinary DFs.
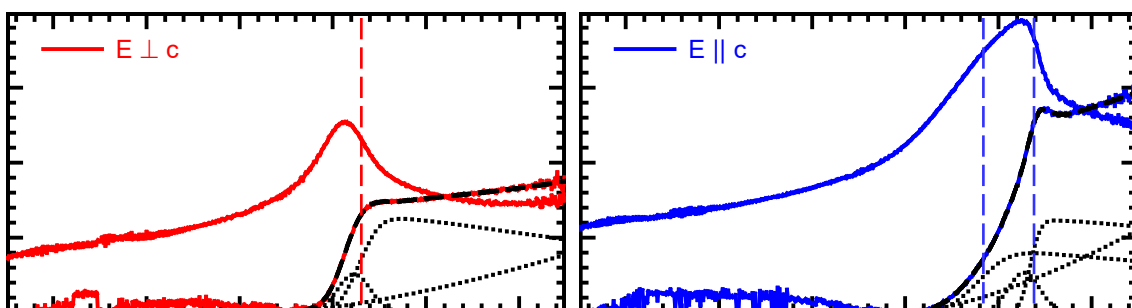
Fig. 3: *Ordinary (left) and extraordinary (right) DFs of the bulk sample. [6] The point-by-point fitted DFs are shown as continuous curves. Black dashed curves represent the fit by exciton model to the imaginary parts. The single components of the fits are shown as dotted curves. Characteristic transition energies are indicated by vertical dashed lines.*

In the next step, Sb-doped MBE-grown (101) layers with n up to $2.6*10^{20}$ cm^{-3} where studied and analyzed in the same way. We find a systematic shift of the absorption onsets to higher photon energies with increasing carrier concentrations (Fig. 4). This is explained by the interplay of the many body effects bandgap renormalization and conduction-band filling leading finally to an effective Burstein-Moss shift. The extraordinary absorption edge undergoes a continuous change in shape with increasing n, the low-energy feature becomes clearly visible (marked by an arrow in the lower left panel of Fig. 4). It emphasizes for this light polarization the superposition of transitions from two valence bands with different curvature (hole masses) into the partly filled CB.
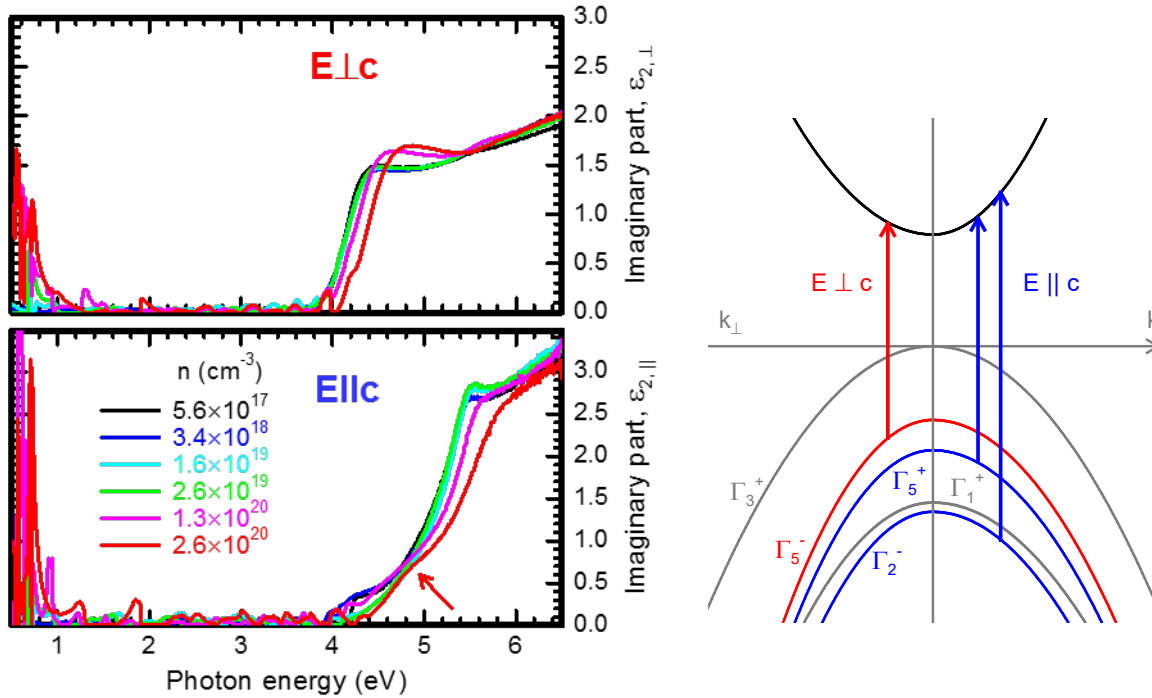
Fig. 4: Left: Point-by-point fitted imaginary parts of the ordinary (upper) and extraordinary (lower) DFs for increasing free-electron concentrations. The additional low energy feature found in the extraordinary dielectric function is marked by an arrow. Right: Sketched band diagram around the center of the Brillouin zone. The optically observed transitions are marked as vertical arrows. Special emphasis is laid on the valence band offsets which are deduced quantitatively from the extrapolation of the absorption edges to zero free electrons. [6]
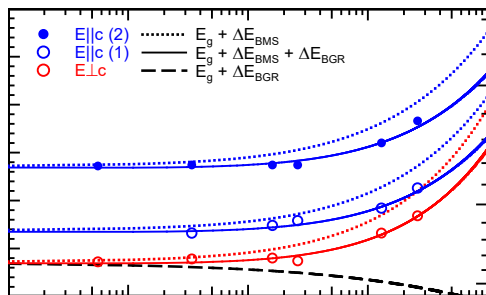
Fig 5: Energies of the bandgaps for all observed transitions in both polarization directions of the electric field vector (symbols) as a function of electron concentration. Dotted curves symbolize the contribution of the Burstein-Moss shift only, dashed is the bandgap renormalization, continuous curves are the sum of both effects. [6]

The fit of the DFs in Fig. 4 with appropriate analytical models yields the characteristic transition energies for the two polarization directions which are plotted in Fig. 5 as a function of electron density. A quantitative analysis relies on (i) the calculation of the bandgap renormalization, (ii) a correct description of effective electron mass anisotropies, (iii) a new approach for describing the CB nonparabolicity, and (iv) finally literature values for hole masses of $1.21*m_0$ and $1.47*m_0$ perpendicular and parallel to the **c**-axis, respectively, as described in detail in

reference 6. The excellent overall agreement is clearly visible. The energy differences for low n mirror the splitting between valence bands with the symmetries indicated in Fig. 4.

In summary, electrical and optical studies of SnO_2 bulk crystals and MBE-grown thin layers revealed a pronounced anisotropy of the corresponding properties being related to the rutile crystal structure. The anisotropy and nonparabolicity of the conduction band is the key point for the interpretation of the data. With these data, we are able to experimentally access valence band properties like valence band splittings and anisotropic hole masses in heavily n-type doped samples. [6]

[1]   M. Feneberg, C. Lidig, K. Lange, M.E. White, M.Y. Tsai, J.S. Speck, O. Bierwagen, and R. Goldhahn,
Anisotropy of the electron effective mass in rutile SnO_2 determined by infrared ellipsometry,
Phys. Status Solidi A **211**, 82 (2014). DOI: 10.1002/pssa.201330147

[2]   Z. Galazka, R. Uecker, D. Klimm, K. Irmscher, M. Pietsch, R. Schewski, M. Albrecht, A. Kwasniewski, S. Ganschow,
D. Schulz, C. Guguschev, R. Bertram, M. Bickermann, and R. Fornari,
Growth, characterization, and properties of bulk SnO_2 single crystals,
Phys. Status Solidi A **211**, 66 (2014). DOI: 10.1002/pssa.201330020

[3]   M. E. White, O. Bierwagen, M. Y. Tsai, and J. S. Speck,
Electron transport properties of antimony doped SnO_2 single crystalline thin films grown by plasma-assisted
molecular beam epitaxy,
J. Appl. Phys. **106**, 093704 (2009). DOI: 10.1063/1.3254241

* [4]   O. Bierwagen and Z. Galazka,
The inherent transport anisotropy of rutile tin dioxide (SnO_2) determined by van der Pauw measurements and its
consequences for applications,
Appl. Phys. Lett. **112**, 092105 (2018). DOI: 10.1063/1.5018983

[5]   M. Feneberg, C. Lidig, K. Lange, R. Goldhahn, M.D. Neumann, N. Esser, O. Bierwagen, M.E. White, M.Y. Tsai,
and J.S. Speck,
Ordinary and extraordinary dielectric functions of rutile SnO_2 up to 20 eV,
Appl. Phys. Lett. **104**, 231106 (2014). DOI: 10.1063/1.4882237

* [6]   M. Feneberg, C. Lidig, M.E. White, M.Y. Tsai, J.S. Speck, O. Bierwagen, Z. Galazka, and R. Goldhahn,
Anisotropic optical properties of highly doped rutile SnO_2: Valence band contributions to the Burstein-Moss shift,
APL Materials **7**, 022508 (2019). DOI: 10.1063/1.5054351

GraFox publications are highlighted by an "*".